Blackbody-radiation-noise broadening of quantum systems

Eric B. Norrgard [1,*] Stephen P. Eckel [1] Christopher L. Holloway [2] and Eric L. Shirley [1]
[1]*Sensor Science Division, National Institute of Standards and Technology, Gaithersburg, Maryland 20899, USA*
[2]*RF Technology Division, National Institute of Standards and Technology (NIST), Boulder, Colorado 80305, USA*

(Received 8 January 2021; accepted 17 March 2021; published 5 April 2021)

Precision measurements of quantum systems often seek to probe or must account for the interaction with blackbody radiation. Over the past several decades, much attention has been given to ac Stark shifts and stimulated state transfer. For a blackbody in thermodynamic equilibrium, these two effects are determined by the expectation value of photon number in each mode of the Planck spectrum. Here we explore how the photon number variance of an equilibrium blackbody generally leads to a parametric broadening of the energy levels of quantum systems that is inversely proportional to the square root of the blackbody volume. We consider the effect in two cases which are potentially highly sensitive to this broadening: Rydberg atoms and atomic clocks. We find that even in blackbody volumes as small as 1 cm^3, this effect is unlikely to contribute meaningfully to transition linewidths.

DOI: 10.1103/PhysRevA.103.042806

I. INTRODUCTION

Precision spectroscopy of atomic and molecular systems is the basis of numerous metrological applications [1,2] and tests of fundamental physics [3,4] and symmetries [5,6]. A correct determination of transition energies requires careful accounting of Stark shifts due to ambient blackbody radiation (BBR). High-accuracy BBR shift calculations account for higher order electric and magnetic multipolar moments [7] in the scalar and tensor light shifts [8,9]. For optical lattice clocks, shifts induced by the trapping laser must also be considered to attain high accuracy (including shifts which are quadratic and higher order in electromagnetic field energy density, known as hyperpolarizability) [10].

In addition to shifting energy levels, blackbody radiation can drive transitions to other levels. This effect can be considered a nonparametric line broadening, as the BBR-stimulated transition rate Γ^{BBR} adds to the spontaneous decay rate Γ^{sp} [11]. BBR-stimulated decay is prominent in Rydberg atomic systems (typically $\Gamma^{\mathrm{BBR}} \gtrsim 10^4$ s^{-1} at room temperature), and has also been observed in trapped molecules [12,13], and molecular ions [14].

Recently we surveyed the BBR-induced state transfer and levels shifts in molecular and atomic Rydberg systems, showing these are highly promising platforms for blackbody thermometry applications [2]. That work led us to consider the potential impacts of line broadening due to temporal fluctuations in the BBR. However, this additional BBR-induced line broadening mechanism appears to have been overlooked until now. For a blackbody at temperature T encompassing a volume V, fluctuations in the BBR energy produce a root-mean-square (RMS) deviation $\sigma_{\Delta E_i}$ in the BBR shift ΔE_i. The broadening is proportional to $\sqrt{T^5/V}$ when the energy differences $\hbar\omega_{ij}$ associated with strongest transitions are all large compared to the thermal energy scale (i.e., $\hbar\omega_{ij} \gg k_{\mathrm{B}}T$). Unlike BBR-stimulated transitions, the BBR noise induces a parametric broadening (i.e., the quantum state remains unchanged). This effect is general to all quantum systems which are radiatively coupled to a thermal bath.

Here we derive the effect of BBR noise on a quantum system. As we show below, the BBR noise broadening is inconsequentially small for typical atom or molecule and will not be detectable in Rydberg or molecule-based BBR thermometry applications [2]. We consider in detail the size of the effect on two systems which are exceptionally sensitive to BBR noise broadening: atomic clocks and circular Rydberg atoms. For both systems, we find the BBR noise is still too small to significantly contribute to line broadening under any currently feasible scenario. The present work thus serves to consider this effect in detail, as well as noting that it may safely be ignored, even by many precision measurements.

II. BACKGROUND

A. Photon statistics

Before deriving the BBR noise broadening, we summarize the relevant photon statistics and ac Stark interaction (see Appendix A for more details on photon statistics). For photons with angular frequency ω, we will use $x = \hbar\omega/k_BT$ to write the partition function $Z = (1 - e^{-x})^{-1}$. The mth moment of the photon number n is

$$\langle \hat{n}^m \rangle = \frac{1}{Z}\sum_{n=0}^{\infty} n^m e^{-nx} = \frac{1}{Z}\frac{\partial^m}{\partial(-x)^m} Z(x). \tag{1}$$

The variance in photon number for each BBR mode is $\sigma_{\hat{n}}^2 = \langle \hat{n}^2 \rangle - \langle \hat{n} \rangle^2 = e^x/(e^x - 1)^2$. In this work, a hat over a symbol indicates an operator.

*eric.norrgard@nist.gov

We consider an ideal blackbody of effective volume V and temperature T which surrounds a quantum system in state i. In this work, we define the effective length ℓ and volume V of the cavity through the mode spacing. Physically, a blackbody cavity is created through a combination of a resistive wall material, light trapping geometry [15], and surface micro-structure [16,17]. A plane wave incident on a surface with nonzero resistance incurs a phase shift according to the Fresnel equations. Effectively, these phase shifts increase the cavity size and decrease the mode spacing compared to that of an ideal conductor. Similarly, surface microstructure can increase the physical length of each incident mode. For this work, we will not concern ourselves with these complications and instead compare cavities with equal effective size—that is, cavities with identical mode spacing—rather than cavities with equal physical dimensions.

B. ac Stark interaction

The ac Stark interaction has received considerable attention [18–21]. It is characterized by a real and an imaginary contribution [20–23], and the instantaneous values of both contributions fluctuate due to fluctuations in the occupancy of all photon modes. On the average, the interaction is given by

$$\left\langle \mathscr{E}_i^{\mathrm{BBR}} \right\rangle = \langle \Delta E_i \rangle - \frac{i\hbar}{2}\left\langle \Gamma_i^{\mathrm{BBR}} \right\rangle = -\int_0^\infty d\omega \frac{\langle \hat{\mathcal{E}}^2 \rangle}{2} \alpha_i^s(\omega), \quad (2)$$

where $\hat{\mathcal{E}}$ is the electric field operator, and $\alpha_i^s(\omega)$ is the scalar polarizability of level i:

$$\alpha_i^s(\omega) = \sum_j \frac{\left|\mu_{ij}^z\right|^2}{\hbar}\left(\frac{1}{\omega_{ij} - \omega - \frac{i}{2}\Gamma_j^{\mathrm{sp}}} + \frac{1}{\omega_{ij} + \omega + \frac{i}{2}\Gamma_j^{\mathrm{sp}}}\right). \quad (3)$$

Here μ_{ij}^z is the z component of the dipole matrix element between states i and j, and Γ_j^{sp} is the spontaneous decay rate of level j.

The expectation value of the imaginary part $\langle \Gamma_i^{\mathrm{BBR}} \rangle$ of Eq. (2) is associated with stimulated state transfer from level i to other levels j of the system:

$$\left\langle \Gamma_i^{\mathrm{BBR}} \right\rangle = \sum_j \frac{\left|\mu_{ij}^z\right|^2 |\omega_{ij}|^3}{\varepsilon_0 \hbar \pi c^3} \langle \hat{n}(\omega_{ij}) \rangle. \quad (4)$$

The average real part of Eq. (2) is a shift in the energy of level i, given by [11,24]

$$\langle \Delta E_i \rangle = -P\int_0^\infty d\omega \frac{\hbar\omega^3 \langle \hat{n}(\omega) \rangle}{2\varepsilon_0 \pi^2 c^3} \alpha_i^s(\omega), \quad (5)$$

where P denotes the Cauchy principal value. For brevity, in the remainder of this work we shall drop the angled brackets so that ΔE_i and $\Gamma_i{}^{\mathrm{BBR}}$ are to be interpreted as expectation values, and the frequency dependence of $\hat{n}$ will be made implicit.

III. BLACKBODY RADIATION NOISE

In the absence of other broadening mechanisms, the interaction of a quantum system with the mean BBR field leads to a Lorentzian line shape with full width at half maximum (FWHM):

$$\Gamma_i = \Gamma_i^{\mathrm{sp}} + \Gamma_i^{\mathrm{BBR}}. \quad (6)$$

Here we seek to quantify the small, additional broadening of the quantum level induced by fluctuations in the BBR electric field. These fluctuations lead to RMS deviations $\sigma_{\Delta E_i}$ in the ac Stark shift ΔE_i. These fluctuations occur with typical timescale of the blackbody coherence time $t_c = h/4k_{\mathrm{B}}T$ ($t_c \approx$ 40 fs at room temperature) [25]. Therefore, the expected line shape for a single measurement with duration $t_m \gg t_c$ is a Voigt profile with Lorentzian width $\gamma = \Gamma_i$ and Gaussian half width at half maximum (HWHM) $\sigma = \sigma_{\Delta E_i}\sqrt{t_c/t_m}$. The FWHM of a Voigt profile is approximately

$$\mathrm{FWHM_V} \approx \frac{\gamma}{2} + \sqrt{\frac{\gamma^2}{4} + 8\sigma^2 \ln 2}. \quad (7)$$

In the limit $\gamma \gg \sigma$, the Voigt FWHM becomes

$$\mathrm{FWHM_V} \approx \gamma + 8\ln 2 \frac{\sigma^2}{\gamma}. \quad (8)$$

In order to calculate $\sigma_{\Delta E_i}$, we begin by considering each photon mode as contributing $\Delta\epsilon_i$ to the total shift, i.e., $\Delta E_i = \sum_{\mathrm{modes}} \Delta\epsilon_i$. Assuming uncorrelated modes, $\sigma_{\Delta E_i}^2 = \sum_{\mathrm{modes}} \sigma_{\Delta\epsilon_i}^2$, it suffices to find the contribution of each mode independently. The summation $\sum_{\mathrm{modes}}$ corresponds to $P\int V D_{\mathrm{mode}}$ in the continuous limit, where D_{mode} is the density of modes per unit volume per unit angular frequency $d\omega$, and $D_{\mathrm{mode}} = D_{\mathrm{mode}}^{\mathrm{FS}} = \omega^2 d\omega/\pi^2 c^3$ for free space. Combining this with Eq. (5) yields

$$\Delta\epsilon_i = -\frac{\hbar\omega\langle\hat{n}\rangle}{2\varepsilon_0 V}\alpha_i^s(\omega), \quad (9)$$

and the variance of the shift is given by

$$\sigma_{\Delta\epsilon_i}^2 = \left|\frac{\partial\Delta\epsilon_i}{\partial\hat{n}}\right|^2 \sigma_{\hat{n}}^2 = \left|\frac{\hbar\omega}{2\varepsilon_0 V}\alpha_i^s(\omega)\right|^2 \sigma_{\hat{n}}^2. \quad (10)$$

Finally we add the contributions of each mode in quadrature to arrive at the variance of the ac Stark shift due to BBR noise:

$$\begin{aligned}\sigma_{\Delta E_i}^2 &= \sum_{\mathrm{modes}} \sigma_{\Delta\epsilon_i}^2 \\ &= P\int_0^\infty V D_{\mathrm{mode}} \frac{\hbar^2\omega^2\sigma_{\hat{n}}^2}{4\varepsilon_0^2 V^2}\left|\alpha_i^s(\omega)\right|^2 \\ &= P\int_0^\infty d\omega \frac{\hbar^2\omega^4}{4\varepsilon_0^2\pi^2 c^3 V}\frac{e^{\hbar\omega/k_{\mathrm{B}}T}}{(e^{\hbar\omega/k_{\mathrm{B}}T}-1)^2} \\ &\quad \times \left|\sum_j \frac{1}{\hbar}\left(\frac{\left|\mu_{ij}^z\right|^2}{\omega_{ij} - \omega - \frac{i}{2}\Gamma_j^{\mathrm{sp}}} + \frac{\left|\mu_{ij}^z\right|^2}{\omega_{ij} + \omega + \frac{i}{2}\Gamma_j^{\mathrm{sp}}}\right)\right|^2, \end{aligned} \quad (11)$$

where in the last line we take $D_{\mathrm{mode}} = D_{\mathrm{mode}}^{\mathrm{FS}}$. Note that the summation within the modulus in Eq. (11) is identical to that found in the Kramers-Heisenberg formula for differential scattering cross section of light (e.g., Ref. [32] Sec. 8.7; also Ref. [22]); that is, we can consider the BBR noise broadening of each level i to be due to variance in BBR Rayleigh scattering rate due to fluctuating photon number in each mode. Also

of note is the RMS fluctuation in the BBR shift $\sigma_{\Delta E_i}$ is proportional to $1/\sqrt{V}$. While the RMS electric field of a blackbody is independent of volume, smaller volumes contain fewer modes which contribute to the field, and thus are subject to larger field variations. This relationship between BBR fluctuations and volume was first noted by Einstein [33], and Eq. (11) can alternately be derived using standard thermodynamic relations (see Appendix B).

Often the quantum observable of interest is not the ac Stark shift, but the differential ac Stark shift $\Delta E'_{ij} = \Delta E_j - \Delta E_i$, such as when measuring the transition frequency ω_{ij} between two states i, j. Conventionally, negative shifts imply a decrease in the observed transition frequency. Likewise, for the BBR noise line broadening, we define the differential shift per mode $\Delta\epsilon'_{ij} = \Delta\epsilon_j - \Delta\epsilon_i$:

$$\Delta\epsilon'_{ij} = \frac{\hbar\omega\langle\hat{n}\rangle}{2\varepsilon_0 V}\alpha^{s\,\prime}_{ij}(\omega) \tag{12}$$

with $\alpha^{s\,\prime}_{ij}(\omega) = \alpha^s_j(\omega) - \alpha^s_i(\omega)$ the differential dynamic scalar polarizability.

In many cases, is it appropriate to make a static approximation $y_{ij} = \hbar\omega_{ij}/k_B T \gg 1$. In this limit,

$$\Delta E'_{ij} = \frac{\hbar}{2\varepsilon_0\pi^2 c^3}\frac{\pi^4}{15}\left(\frac{k_B T}{\hbar}\right)^4 \alpha^{s\,\prime}_{ij}(0), \tag{13}$$

$$\sigma^2_{\Delta E'_{ij}} = \frac{\hbar^2}{4\varepsilon_0^2\pi^2 c^3 V}\frac{4\pi^4}{15}\left(\frac{k_B T}{\hbar}\right)^5 \left|\alpha^{s\,\prime}_{ij}(0)\right|^2, \tag{14}$$

where we have used the identities

$$\int_0^\infty dx \frac{x^3}{e^x - 1} = \frac{\pi^4}{15}, \quad \int_0^\infty dx \frac{x^4 e^x}{(e^x - 1)^2} = \frac{4\pi^4}{15}. \tag{15}$$

To the best of our knowledge, the BBR noise broadening effect described by Eq. (11) has not been observed experimentally. That is unsurprising, as in most cases, this effect is quite small. Consider, for example, an atomic transition with $y_{ij} \gg 1$ and differential polarizability $\alpha^{s\,\prime}_{ij}(0) = (4\pi\varepsilon_0/h) \times 1\, a_0^3$ (where $a_0 \approx 52.9$ pm is the Bohr radius), then $\sigma = \sigma_{\Delta E'_{ij}}\sqrt{t_c/t_m} \approx 3.0 \times 10^{-16}\sqrt{t_c T^5/t_m V}$ Hz m$^{3/2}$ K$^{-5/2}$. For $T = 300$ K and $V = 1$ L $= 10^{-3}$ m^3, $\sigma_{\Delta E'_{ij}} \approx h \times 14$ nHz. In nearly all practical measurements, the fluctuation $\sigma = \sigma_{\Delta E'_{ij}}\sqrt{t_c/t_m}$ averages down the numerically small value of $\sigma_{\Delta E'_{ij}}$ by a considerable factor (e.g., for $t_m = 1$ s, $\sqrt{t_c/t_m} \approx 2 \times 10^{-7}$ at room temperature). We then see using Eq. (8) that the BBR noise broadening becomes a vanishingly small correction to the linewidth ($\sigma \approx 3$ fHz in this example).

For the Cs hyperfine transition, which currently defines the second, the BBR noise broadening is even smaller. The differential scalar polarizability $\alpha^{s\,\prime}_{ij}(0) \approx (4\pi\varepsilon_0/h) \times 0.0069\, a_0^3$ [34] is predominantly due to coupling at optical frequencies to the first few electronically excited P states, so Eqs. (13) and (14) are valid. If $T = 300$ K and $V = 1$ L, then $\sigma \approx h\sqrt{t_c/t_m} \times 700$ fHz.

We detail below two special cases where BBR noise broadening might be most noticeable: optical atomic clocks and circular Rydberg atoms. However, we find in both cases the BBR noise is too small to be detected with modern experimental techniques.

A. Optical atomic frequency standards

In Table I we consider several current and proposed atomic frequency standards at $T = 300$ K. We calculate the RMS differential BBR shift deviation $\sigma_{\Delta E'_{ij}}$ using Eq. (14) as well as the differential BBR Stark shift $\Delta E'_{ij}$ using Eq. (13) as a check of consistency with the atomic transition data references [18,29–31]. For the BBR shift of optical clock transitions, the static approximation is generally accurate to within a few percent [18]. Differential polarizablities in Table I are given in their respective references in atomic polarizability units. These may be converted to SI units (Hz/(V/m)^2) by multiplying by a factor of $4\pi\varepsilon_0 a_0^3/h$, with a_0 the Bohr radius.

The results of Table I show that detection of BBR noise broadening in atomic frequency standards is not possible without several orders of magnitude improvement over current frequency sensitivity. Consider as examples the Sr and Yb systems, which now routinely achieve fractional uncertainty of $\delta\omega/\omega \sim 10^{-18}$ [35–37]. Ignoring numerous technical noise sources (e.g., lattice phonon scattering in optical lattice clocks [38]), even in an exceptionally small BBR volume $V = 10^{-6}$ m^3 at $T = 300$ K, $\sigma_{\Delta E'_{ij}}$ is only approximately 30 mHz in Sr and 10 mHz in Yb. For a measurement time $t_m = 1$ s, the BBR noise broadening is then $\sigma \approx 6$ nHz for Sr and $\sigma \approx 2$ nHz for Yb. Using Eq. (8), the observed FWHM would then exceed $\Gamma^{\rm sp}$ by approximately $(1 \times 10^{-10})\Gamma^{\rm sp}$ for Sr, or $(4 \times 10^{-13})\Gamma^{\rm sp}$ for Yb. The small differential polarizability characteristic of ions [18,26,29], inner-shell transitions [28,29], and the nuclear transition of ^{229}Th [30,31] makes the BBR noise broadening in these systems even smaller than the Sr and Yb cases. We note that effective BBR volumes V substantially less than 10^{-6} m^3 might be possible using microfabricated optical cavities [39].

B. Circular Rydberg atoms

We next consider the possibility of observing BBR noise-limited linewidths in circular Rydberg states $|n\mathrm{C}\rangle \equiv |n, L = n-1, J = n-1/2\rangle$. It is well known that all Rydberg systems with large principal quantum number n may be approximated by a Rydberg hydrogen atom with an appropriate quantum defect (e.g., see Ref. [40] for Rb quantum defects). For concreteness, we here use the Alkali Rydberg Calculator python package [41] to calculate transition matrix elements and energies for circular states of Rb. The largest transition dipole matrix elements for Rydberg atoms with principal quantum number n are to states with $n' = n \pm 1$. For our circular Rydberg state calculations, we include electric dipole transitions to $n' = n-1, n+1, n+2, n+3$.

Rydberg transition wavelengths may be as large or larger than the length scale of its surroundings, and we must consider cavity effects on the mode density $D_{\rm mode}$. Figure 1 shows $\sigma_{\Delta E_i}$ for the $|52\mathrm{C}\rangle$ state of Rb in an effective cubic volume $V = \ell^3$ for three key conceptual cases. The dashed colored lines depict $\sigma_{\Delta E_i}$ calculated using $D_{\rm mode} = D^{\rm FS}_{\rm mode}$; in this case $\sigma_{\Delta E_i}$ is strictly proportional to $\ell^{-3/2}$. The solid black line depicts an ideal blackbody (i.e., perfectly absorbing walls); the mode density for a blackbody $D^{\rm BB}_{\rm mode}$ is found by quantizing the cavity modes in the usual manner and assigning

TABLE I. BBR Stark shifts and noise broadening for optical clock systems. All temperature-dependent quantities are evaluated at $T = 300$ K. Static differential polarizabilities $\alpha_{ij}^{s}{}'(0)$ from Ref. [18] are the recommended calculated value or mean of values when multiple calculations using the highest accuracy method were presented. For measurement time t_m, the BBR noise broadening is $\sigma = \sigma_{\Delta E'_{ij}}\sqrt{t_c/t_m}$.

						$(V = 10^{-3}\ \mathrm{m}^3)$		$(V = 10^{-6}\ \mathrm{m}^3)$	
	ν_{ij} (PHz)	y_{ij}	Γ^{sp} (Hz)	$\alpha_{ij}^{s}{}'(0)$ (a_0^3)	$\Delta E'_{ij}$ (Hz)	$\sigma_{\Delta E'_{ij}}$ (Hz)	$\sigma_{\Delta E'_{ij}}/\Gamma^{\mathrm{sp}}$	$\sigma_{\Delta E'_{ij}}$ (Hz)	$\sigma_{\Delta E'_{ij}}/\Gamma^{\mathrm{sp}}$
Ca^+ [18]	0.411	65.7	1.4×10^{-1}	−44.1	3.8×10^{-1}	2.75×10^{-5}	1.97×10^{-4}	8.71×10^{-4}	6.22×10^{-3}
Sr^+ [18]	0.445	71.2	4.0×10^{-1}	−29.3	2.5×10^{-1}	1.22×10^{-5}	3.04×10^{-5}	3.84×10^{-4}	9.61×10^{-4}
Yb^{+a} [18]	0.642	102.7	1.0×10^{-9}	9.3	-8.0×10^{-2}	1.22×10^{-6}	1.22×10^{3}	3.87×10^{-5}	3.87×10^{4}
Yb^{+b} [18]	0.688	110.1	3.1	42	-3.6×10^{-1}	2.50×10^{-5}	8.06×10^{-6}	7.90×10^{-4}	2.55×10^{-4}
Al^+ [18]	1.121	179.3	8.0×10^{-3}	0.483	-4.2×10^{-3}	3.30×10^{-9}	4.13×10^{-7}	1.04×10^{-7}	1.31×10^{-5}
In^+ [18]	1.27	203.2	8.0×10^{-1}	<30.7	$>-2.6\times10^{-1}$	$<1.33\times10^{-5}$	$<1.67\times10^{-5}$	$<4.22\times10^{-4}$	$<5.27\times10^{-4}$
Lu^+ [26,27]	0.354	56.6	5.1×10^{-6}	0.059	−0.00051	4.93×10^{-11}	9.59×10^{-6}	1.56×10^{-9}	0.00030
Mg [18]	0.655	104.8	1.4×10^{-4}	29.9	-2.6×10^{-1}	1.27×10^{-5}	9.04×10^{-2}	4.00×10^{-4}	2.86
Ca [18]	0.454	72.6	5.0×10^{-4}	133.2	−1.15	2.51×10^{-4}	5.02×10^{-1}	7.94×10^{-3}	1.59×10^{1}
Sr [18]	0.429	68.6	1.4×10^{-3}	261.1	−2.3	9.65×10^{-4}	6.89×10^{-1}	3.05×10^{-2}	2.18×10^{1}
Yb [18]	0.518	82.9	8.0×10^{-3}	155	−1.33	3.40×10^{-4}	4.25×10^{-2}	1.08×10^{-2}	1.34
Zn [18]	0.969	155.0	2.5×10^{-3}	29.57	-2.6×10^{-1}	1.24×10^{-5}	4.95×10^{-3}	3.91×10^{-4}	1.57×10^{-1}
Cd [18]	0.903	144.5	1.0×10^{-2}	30.66	-2.6×10^{-1}	1.33×10^{-5}	1.33×10^{-3}	4.21×10^{-4}	4.21×10^{-2}
Hg [18]	1.129	180.6	1.1×10^{-1}	21	-1.81×10^{-1}	6.24×10^{-6}	5.68×10^{-5}	1.97×10^{-4}	1.80×10^{-3}
Tm [28]	0.263	42.1	1.2	−0.063	5.4×10^{-4}	5.62×10^{-11}	4.68×10^{-11}	1.78×10^{-9}	1.48×10^{-9}
W^{13+} [29]	0.539	86.2	1.5×10^{1}	−0.024	2.1×10^{-4}	8.16×10^{-12}	5.54×10^{-13}	2.58×10^{-10}	1.75×10^{-11}
Ir^{16+} [29]	0.750	120.0	4.0×10^{1}	−0.01	8.6×10^{-5}	1.42×10^{-12}	3.59×10^{-14}	4.48×10^{-11}	1.13×10^{-12}
Pt^{17+} [29]	0.745	119.2	3.9×10^{-11}	0.182	-1.57×10^{-3}	4.69×10^{-10}	1.19×10^{1}	1.48×10^{-8}	3.77×10^{2}
^{229}Th [30,31]	2.002	319.9	6.3×10^{-3}	$<4\times10^{-5}$	$>-3.4\times10^{-7}$	$<2.27\times10^{-17}$	$<3.61\times10^{-15}$	$<7.16\times10^{-16}$	$<1.14\times10^{-13}$

[a] $-4f^{14}6s - 4f^{13}6s^2\ {}^2F_{7/2}$.
[b] $-4f^{14}6s - 4f^{14}5d\ {}^2D_{3/2}$.

each mode a finesse $\mathscr{F} = 1/4$ (see Appendix C for additional details on cavity effects on mode density). Finally, solid colored lines depict a cubic copper cavity. The mode density for copper $D_{\mathrm{mode}}^{\mathrm{Cu}}$ is complicated by the fact that the resistivity ρ of cryogenic copper may vary by two orders of magnitude depending on purity [42]; we assume residual-resistance ratios typical of oxygen-free high conductivity Cu: $\rho(T = 300\,\mathrm{K})/\rho(\mathrm{T} = 77\,\mathrm{K}) = 10$ and $\rho(T = 300\,\mathrm{K})/\rho(\mathrm{T} = 4\,\mathrm{K}) = 100$, with $\rho(T = 300\,\mathrm{K}) = 1.7\times10^{-8}\ \Omega\,\mathrm{m}$.

Figure 2 considers Rb circular states for principal quantum number $n \leqslant 80$ in a cubic ideal blackbody. The black dashed lines depict the Lorentzian partial linewidth due to spontaneous decay Γ_i^{sp}. Colored dashed lines depict the partial linewidth due to both spontaneous and BBR-stimulated decay $\Gamma_i = \Gamma_i^{\mathrm{sp}} + \Gamma_i^{\mathrm{BBR}}$. Solid lines depict BBR noise Gaussian width $\sigma_{\Delta E_i}\sqrt{t_c\Gamma_i}$, where we have assumed a measurement time $t_m = 1/\Gamma_i$. The magnitude of the BBR noise relative to the decay rate is increased in cryogenic environments, as $\sigma_{\Delta E_i}$ decreases more slowly than $\Gamma_i^{\mathrm{sp}} + \Gamma_i^{\mathrm{BBR}}$ with decreasing temperature. For effective volumes $V = 1\ \mathrm{m}^3$, $\sigma_{\Delta E_i}$ is smaller than Γ_i by roughly six orders of magnitude, even at $T = 4$ K and $n = 80$. For blackbodies with $V = 10^{-6}\ \mathrm{m}^3$, $\sigma_{\Delta E_i}$ is smaller than Γ_i by roughly two orders of magnitude at $T = 4$ K and $n = 80$. We caution that for such large n, typical relevant transition wavelengths are similar to or exceed $\ell = 1$ cm for this case. The assumption of an ideal blackbody for high n and small V is likely invalid, with the BBR noise reduced from these estimates by one or more orders of mag-

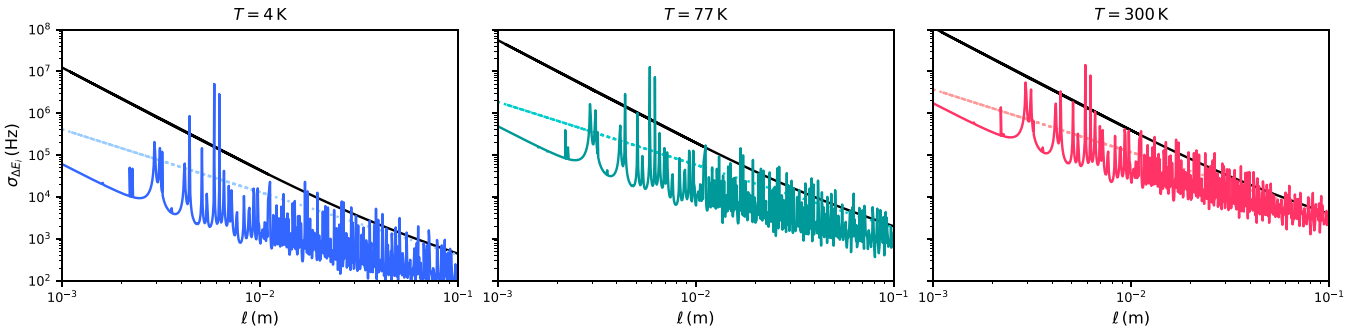

FIG. 1. Blackbody radiation noise $\sigma_{\Delta E_i}$ as a function of the length ℓ of a cubic cavity. From left to right, panels show the circular state of Rb with principal quantum number $n = 52$ for cavity temperature 4 K, 77 K, and 300 K, respectively. The dashed, solid black, and solid colored lines calculate $\sigma_{\Delta E_i}$ with the density of modes D_{mode} equal to free space, perfectly absorbing walls, and copper walls, respectively.

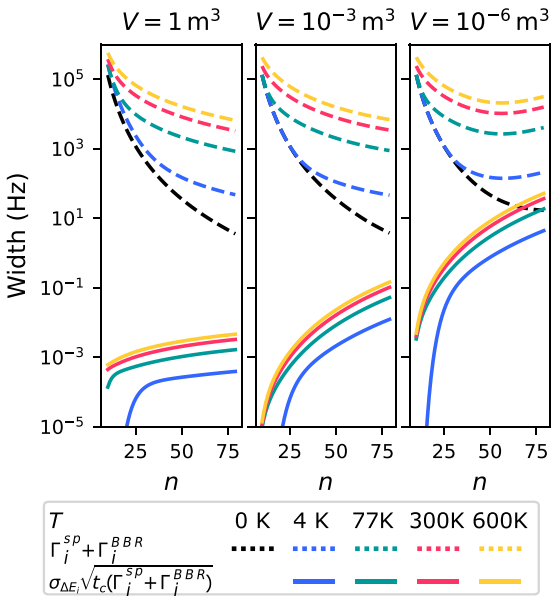

FIG. 2. Decay rate $\Gamma^{\mathrm{sp}} + \Gamma^{\mathrm{BBR}}$ (dashed lines) and blackbody radiation noise $\sigma_{\Delta E_i}\sqrt{t_c(\Gamma^{\mathrm{sp}} + \Gamma^{\mathrm{BBR}})}$ assuming decay rate-limited measurement time (solid lines) for circular states of Rb as a function of principal quantum number n. From left to right, panels show a cubic ideal blackbody with effective volume V of 1 m^3, 10^{-3} m^3, and 10^{-6} m^3, respectively.

nitude as in Fig. 1. The observed FWHM for circular Rydberg states is therefore unlikely to exceed Γ_i by more than roughly $10^{-6} \times \Gamma_i$ in the most favorable cases.

IV. CONCLUSIONS

In this work, we have assumed isotropic polarization of the BBR, and thus considered only the scalar polarizability. As each mode has two independent polarizations, polarization fluctuations in the BBR can lead to broadening which involves the vector and tensor polarizabilities as well. BBR noise broadening due to vector and tensor couplings may be of similar magnitude to scalar couplings in experiments with oriented quantum systems, such as optical lattice clocks or quantum sensing, and could be considered in future work.

We have derived a parametric broadening, general to all quantum systems, which is due to interactions with fluctuations in a blackbody radiation field. This BBR noise broadening is most significant in applications which involve small effective BBR volumes, large transition dipole moments, and/or high frequency precision. However, our presented calculations for several atomic clock transitions and for circular Rydberg states of Rb show that BBR noise broadening is typically too small to be detected in these systems with modern sensitivity by at least several orders of magnitude. These calculations catalog a quantum noise source as being well below current sensitivity for many ongoing experiments, such as atomic frequency standards and quantum sensing experiments using circular Rydberg atoms. For future experiments with substantially improved frequency precision, this work also sets a benchmark for testing fundamental thermodynamics of photons.

ACKNOWLEDGMENTS

The authors thank Dazhen Gu, Andrew Ludlow, Kyle Beloy, Michael Moldover, Marianna Safronova, Clément Sayrin, Wes Tew, and Howard Yoon for insightful conversations, and thank Nikunjkumar Prajapati, Joe Rice, and Wes Tew for careful reading of the manuscript.

APPENDIX A: PHOTON STATISTICS

The partition function Z for a blackbody radiation mode with frequency ω is

$$Z = \sum_{n=0}^{\infty} e^{-n\hbar\omega/k_B T} = \frac{1}{1 - e^{-\hbar\omega/k_B T}}. \tag{A1}$$

A standard trick to calculate the mth moment of the photon number n is

$$\langle n^m \rangle = \frac{1}{Z}\sum_{n=0}^{\infty} n^m e^{-nx} = \frac{1}{Z}\frac{\partial^m}{\partial(-x)^m} Z(x). \tag{A2}$$

The first few moments of the photon number are listed in Table II.

APPENDIX B: THERMODYNAMIC DERIVATION

Here we rederive the main result of the main text, Eq. (11), from thermodynamic principles. The total energy $E^{\mathrm{BBR}}(\omega)$ contained within the volume V of a blackbody cavity per unit angular frequency is

$$E^{\mathrm{BBR}}(\omega) = V\frac{\hbar\omega^3}{\pi^2 c^3}\frac{1}{e^{\hbar\omega/k_{\mathrm{B}}T} - 1}. \tag{B1}$$

The variance of $E^{\mathrm{BBR}}(\omega)$ is given by

$$\begin{aligned}\sigma^2_{E^{\mathrm{BBR}}(\omega)} &= k_{\mathrm{B}}T^2\left[\frac{\partial E^{\mathrm{BBR}}(\omega)}{\partial T}\right] \\ &= V\frac{\hbar^2\omega^4}{\pi^2 c^3}\frac{e^{\hbar\omega/k_{\mathrm{B}}T}}{(e^{\hbar\omega/k_{\mathrm{B}}T} - 1)^2} \\ &= V\frac{\hbar^2\omega^4}{\pi^2 c^3}\sigma^2_{n(\omega)}.\end{aligned} \tag{B2}$$

Because the spectral energy density $U(\omega) = \varepsilon_0\mathcal{E}^2 = E^{\mathrm{BBR}}(\omega)/V$, the variance of the spectral energy density is given by

$$\sigma^2_{U(\omega)} = \frac{\hbar^2\omega^4}{V\pi^2 c^3}\sigma^2_{n(\omega)}. \tag{B3}$$

Note that the fluctuations in $U(\omega)$ are inversely proportional to the volume of the cavity.

TABLE II. First four moments of of the photon number n for blackbody radiation, with $x = \hbar\omega/k_B T$.

	$\langle n^m \rangle$
$\langle n \rangle$	$\frac{1}{e^x-1}$
$\langle n^2 \rangle$	$\frac{e^x+1}{(e^x-1)^2}$
$\langle n^3 \rangle$	$\frac{e^{2x}+4e^x+1}{(e^x-1)^3}$
$\langle n^4 \rangle$	$\frac{e^{3x}+11e^{2x}+11e^x+1}{(e^x-1)^4}$

Since

$$\Delta E_i = -\int_0^\infty d\omega \frac{\langle U(\omega)\rangle}{2\varepsilon_0}\alpha_i^s(\omega), \tag{B4}$$

then

$$\sigma^2_{\Delta E_i} = P\int_0^\infty d\omega \left|\frac{\alpha_i^s(\omega)}{2\varepsilon_0}\right|^2 \sigma^2_{U(\omega)}$$
$$= P\int_0^\infty d\omega \frac{\hbar^2\omega^4}{4\varepsilon_0^2 V\pi^2 c^3}\sigma^2_{\hat{n}}|\alpha_i^s(\omega)|^2, \tag{B5}$$

which matches Eq. (11).

APPENDIX C: TREATING A BLACKBODY AS AN OPTICAL CAVITY

Here we derive the characteristic cavity parameters for a blackbody cavity. For a cavity mode of length ℓ, the free spectral range is

$$\Delta f_{\rm FSR} = \frac{c}{2\ell}. \tag{C1}$$

If a photon is emitted into a mode of length ℓ, the characteristic length traveled is precisely ℓ, since blackbodies are by definition perfect absorbers. Therefore, the spectral width of a blackbody cavity mode (Lorentzian HWHM) is

$$\Delta f^{\rm BB}_{\rm cav} = \frac{c}{\ell}. \tag{C2}$$

The finesse of a cavity is defined as $\mathscr{F} = \Delta f_{\rm FSR}/2\Delta f^{\rm BB}_{\rm cav}$. For an ideal blackbody, apparently all modes have a finesse of $\mathscr{F} = 1/4$.

The resonant frequencies of a cubic cavity with side ℓ are $f_q = q\Delta f_{\rm FSR}$. Here $q^2 = q_x^2 + q_y^2 + q_z^2$, and q_x, q_y, q_z are the number of nodes in the x, y, z dimension plus 1, excluding the boundaries. Allowed modes have $q_x, q_y, q_z \geqslant 0$, with at least one of $q_x, q_y, q_z \geqslant 1$. The quality factor of mode q is then $Q \equiv f_q/2\Delta f^{\rm BB}_{\rm cav} = q/4$.

Because each mode of the cavity has a spectral width $\Delta f^{\rm BB}_{\rm cav}$, the spectral density of mode q is

$$d_q(f) = 2\frac{1}{\pi}\frac{f^{\rm BB}_{\rm cav}}{\left(f^{\rm BB}_{\rm cav}\right)^2 + (f_q - f)^2}\,df, \tag{C3}$$

where the prefactor of 2 accounts for two possible polarizations per mode. A related quantity is the "mode density,"

$$D_{\rm mode}(f) = \sum_q d_q(f)/V, \tag{C4}$$

which is the density of modes per unit frequency per unit volume. In the limit of $q \gg 1$, the density of modes is approximately a continuous function

$$D^{\rm FS}_{\rm mode}(f) = \frac{8\pi f^2}{c^3}\,df. \tag{C5}$$

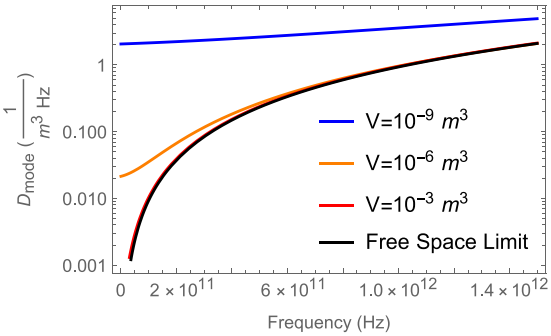

FIG. 3. Density of modes $D_{\rm mode}$ for a perfect absorber as a function of frequency. An excess mode density exists at low frequencies for perfect absorbers compared to free space.

Figure 3 plots $D_{\rm mode}$ of a perfect absorber as a function of frequency f. For finite volume V, there is an excess mode density at low frequencies compared to free space. For real materials, the finesse will generally have a frequency dependence. One can estimate the quality factor by the relation [43]

$$Q = \frac{\text{Energy stored in cavity}}{\text{Energy lost per round trip}} = \frac{3}{2}\frac{V}{S\delta}, \tag{C6}$$

where S is the surface area of the cavity ($S = 6\ell^2$ for a cube) and δ is the skin depth given by [43]

$$\delta = \sqrt{\frac{\varepsilon_0\rho c^2}{\pi f}}. \tag{C7}$$

Here ρ is the material's resistivity and ε_0 is the permittivity of free space. The resistivity ρ is also a frequency dependent parameter but may be approximated by its DC value for sufficiently low frequency. Under this approximation, we find the finesse of a cubic cavity with walls of resistivity ρ is

$$\mathscr{F} = \frac{1}{8\sqrt{\varepsilon_0\rho f/\pi}}. \tag{C8}$$

[1] W. F. McGrew, X. Zhang, R. J. Fasano, S. A. Schäffer, K. Beloy, D. Nicolodi, R. C. Brown, N. Hinkley, G. Milani, M. Schioppo *et al.*, Atomic clock performance enabling geodesy below the centimetre level, Nature (London) **564**, 87 (2018).

[2] E. B. Norrgard, S. P. Eckel, C. L. Holloway, and E. L. Shirley, Quantum blackbody thermometry, New J. Phys. **23**, 033037 (2021).

[3] C. G. Parthey, A. Matveev, J. Alnis, B. Bernhardt, A. Beyer, R. Holzwarth, A. Maistrou, R. Pohl, K. Predehl, T. Udem *et al.*, Improved Measurement of the Hydrogen $1s-2s$ Transition Frequency, Phys. Rev. Lett. **107**, 203001 (2011).

[4] M. S. Safronova, D. Budker, D. DeMille, D. F. J. Kimball, A. Derevianko, and C. W. Clark, Search for new physics with atoms and molecules, Rev. Mod. Phys. **90**, 025008 (2018).

[5] N. Vanhaecke and O. Dulieu, Precision measurements with polar molecules: The role of the black body radiation, Mol. Phys. **105**, 1723 (2007).

[6] M. Ahmadi, B. X. R. Alves, C. J. Baker, W. Bertsche, A. Capra, C. Carruth, C. L. Cesar, M. Charlton, S. Cohen, R. Collister *et al.*, Characterization of the 1S–2S transition in antihydrogen, Nature (London) **557**, 71 (2018).

[7] S. G. Porsev and A. Derevianko, Multipolar theory of blackbody radiation shift of atomic energy levels and its implications for optical lattice clocks, Phys. Rev. A **74**, 020502(R) (2006).

[8] J. Mitroy and M. W. J. Bromley, Dispersion coefficients for H and He interactions with alkali-metal and alkaline-earth-metal atoms, Phys. Rev. A **68**, 062710 (2003).

[9] G. A. Costanzo, S. Micalizio, A. Godone, J. C. Camparo, and F. Levi, ac Stark shift measurements of the clock transition in cold Cs atoms: Scalar and tensor light shifts of the D_2 transition, Phys. Rev. A **93**, 063404 (2016).

[10] R. C. Brown, N. B. Phillips, K. Beloy, W. F. McGrew, M. Schioppo, R. J. Fasano, G. Milani, X. Zhang, N. Hinkley, H. Leopardi *et al.*, Hyperpolarizability and Operational Magic Wavelength in an Optical Lattice Clock, Phys. Rev. Lett. **119**, 253001 (2017).

[11] J. W. Farley and W. H. Wing, Accurate calculation of dynamic Stark shifts and depopulation rates of Rydberg energy levels induced by blackbody radiation. Hydrogen, helium, and alkali-metal atoms, Phys. Rev. A **23**, 2397 (1981).

[12] S. Hoekstra, J. J. Gilijamse, B. Sartakov, N. Vanhaecke, L. Scharfenberg, S. Y. T. van de Meerakker, and G. Meijer, Optical Pumping of Trapped Neutral Molecules by Blackbody Radiation, Phys. Rev. Lett. **98**, 133001 (2007).

[13] H. J. Williams, L. Caldwell, N. J. Fitch, S. Truppe, J. Rodewald, E. A. Hinds, B. E. Sauer, and M. R. Tarbutt, Magnetic Trapping and Coherent Control of Laser-Cooled Molecules, Phys. Rev. Lett. **120**, 163201 (2018).

[14] C. W. Chou, A. L. Collopy, C. Kurz, Y. Lin, M. E. Harding, P. N. Plessow, T. Fortier, S. Diddams, D. Leibfried, and D. R. Leibrandt, Frequency-comb spectroscopy on pure quantum states of a single molecular ion, Science **367**, 1458 (2020).

[15] W. C. Daywitt, The noise temperature of an arbitrarily shaped microwave cavity with application to a set of millimetre wave primary standards, Metrologia **30**, 471 (1994).

[16] E. B. Norrgard, N. Sitaraman, J. F. Barry, D. J. McCarron, M. H. Steinecker, and D. DeMille, In-vacuum scattered light reduction with black cupric oxide surfaces for sensitive fluorescence detection, Rev. Sci. Instrum. **87**, 053119 (2016).

[17] T. Cantat-Moltrecht, R. Cortiñas, B. Ravon, P. Méhaignerie, S. Haroche, J. M. Raimond, M. Favier, M. Brune, and C. Sayrin, Long-lived circular Rydberg states of laser-cooled rubidium atoms in a cryostat, Phys. Rev. Research **2**, 022032(R) (2020).

[18] J. Mitroy, M. S. Safronova, and C. W. Clark, Theory and applications of atomic and ionic polarizabilities, J. Phys. B: At., Mol. Opt. Phys. **43**, 202001 (2010).

[19] V. D. Ovsiannikov, I. L. Glukhov, and E. A. Nekipelov, Ionization cross sections and contributions of continuum to optical characteristics of Rydberg states, J. Phys. B: At., Mol. Opt. Phys. **45**, 095003 (2012).

[20] D. Solovyev, L. Labzowsky, and G. Plunien, QED derivation of the Stark shift and line broadening induced by blackbody radiation, Phys. Rev. A **92**, 022508 (2015).

[21] I. L. Glukhov, A. A. Kamenski, and V. D. Ovsiannikov, The use of oscillator-strength sum rules for evaluating the angular-momentum dependence of the blackbody-radiation-induced broadening and shift of Rydberg-state energy levels, J. Phys. B: At., Mol. Opt. Phys. **53**, 215004 (2020).

[22] F. Low, Natural line shape, Phys. Rev. **88**, 53 (1952).

[23] O. Y. Andreev, L. N. Labzowsky, G. Plunien, and D. A. Solovyev, QED theory of the spectral line profile and its applications to atoms and ions, Phys. Rep. **455**, 135 (2008).

[24] T. F. Gallagher and W. E. Cooke, Interactions of Blackbody Radiation with Atoms, Phys. Rev. Lett. **42**, 835 (1979).

[25] A. Donges, The coherence length of black-body radiation, Eur. J. Phys. **19**, 245 (1998).

[26] E. Paez, K. J. Arnold, E. Hajiyev, S. G. Porsev, V. A. Dzuba, U. I. Safronova, M. S. Safronova, and M. D. Barrett, Atomic properties of Lu^+, Phys. Rev. A **93**, 042112 (2016).

[27] S. G. Porsev, U. I. Safronova, and M. S. Safronova, Clock-related properties of Lu^+, Phys. Rev. A **98**, 022509 (2018).

[28] A. Golovizin, E. Fedorova, D. Tregubov, D. Sukachev, K. Khabarova, V. Sorokin, and N. Kolachevsky, Inner-shell clock transition in atomic thulium with a small blackbody radiation shift, Nat. Commun. **10**, 1724 (2019).

[29] D. K. Nandy and B. K. Sahoo, Highly charged W^{13+}, Ir^{16+}, and Pt^{17+} ions as promising optical clock candidates for probing variations of the fine-structure constant, Phys. Rev. A **94**, 032504 (2016).

[30] C. J. Campbell, A. G. Radnaev, A. Kuzmich, V. A. Dzuba, V. V. Flambaum, and A. Derevianko, Single-Ion Nuclear Clock for Metrology at the 19th Decimal Place, Phys. Rev. Lett. **108**, 120802 (2012).

[31] B. Seiferle, L. von der Wense, P. V. Bilous, I. Amersdorffer, C. Lemell, F. Libisch, S. Stellmer, T. Schumm, C. E. Düllmann, A. Pálffy, and P. G. Thirolf, Energy of the 229th nuclear clock transition, Nature (London) **573**, 243 (2019).

[32] R. Loudon, *The Quantum Theory of Light*, 3rd ed. (Oxford University Press, New York, 2000).

[33] A. Einstein, Zur allgemeinen molekularen Theorie der Wärme, Ann. Phys. **319**, 354 (1904).

[34] S. Micalizio, A. Godone, D. Calonico, F. Levi, and L. Lorini, Blackbody radiation shift of the ^{133}Cs hyperfine transition frequency, Phys. Rev. A **69**, 053401 (2004).

[35] K. Beloy, N. Hinkley, N. B. Phillips, J. A. Sherman, M. Schioppo, J. Lehman, A. Feldman, L. M. Hanssen, C. W. Oates, and A. D. Ludlow, Atomic Clock with 1×10^{-18} Room-Temperature Blackbody Stark Uncertainty, Phys. Rev. Lett. **113**, 260801 (2014).

[36] T. L. Nicholson, S. L. Campbell, R. B. Hutson, G. E. Marti, B. J. Bloom, R. L. McNally, W. Zhang, M. D. Barrett, M. S. Safronova, G. F. Strouse *et al.*, Systematic evaluation of an atomic clock at 2×10^{-18} total uncertainty, Nat. Commun. **6**, 6896 (2015).

[37] I. Ushijima, M. Takamoto, M. Das, T. Ohkubo, and H. Katori, Cryogenic optical lattice clocks, Nat. Photonics **9**, 185 (2015).

[38] S. Dörscher, R. Schwarz, A. Al-Masoudi, S. Falke, U. Sterr, and C. Lisdat, Lattice-induced photon scattering in an optical lattice clock, Phys. Rev. A **97**, 063419 (2018).

[39] M. Trupke, E. A. Hinds, S. Eriksson, E. A. Curtis, Z. Moktadir, E. Kukharenka, and M. Kraft, Microfabricated high-finesse optical cavity with open access and small volume, Appl. Phys. Lett. **87**, 211106 (2005).

[40] W. Li, I. Mourachko, M. W. Noel, and T. F. Gallagher, Millimeter-wave spectroscopy of cold Rb Rydberg atoms in a

magneto-optical trap: Quantum defects of the *ns*, *np*, and *nd* series, Phys. Rev. A **67**, 052502 (2003).

[41] E. J. Robertson, N. Sibalić, R. M. Potvliege, and M. P. A. Jones, Arc 3.0: An expanded python toolbox for atomic physics calculations, Comp. Phys. Commun. **261**, 107814 (2021).

[42] J. W. Ekin, *Experimental Techniques for Low-Temperature Measurements* (Oxford University Press, Oxford, 2006).

[43] B.-H. Liu, D. C. Chang, and M. T. Ma, Eigenmodes and the composite quality factor of a reverberating chamber, NBS Technical Note 1066 (1983).